Multiple Pathways for Mineral Core Formation in Mammalian Apoferritin. The Role of Hydrogen Peroxide†

Guanghua Zhao,‡ Fadi Bou-Abdallah,‡ Paolo Arosio,§ Sonia Levi,|| Christine Janus-Chandler,‡ and N. Dennis Chasteen*,‡

Department of Chemistry, University of New Hampshire, Durham, New Hampshire 03824, Chemistry Section, Faculty of Medicine, University of Brescia, 25123 Brescia, Italy, and IRCCS H. San Raffaele, Protein Engineering Unit, Via Olgettina 58, 20132 Milano, Italy

Received December 12, 2002; Revised Manuscript Received January 21, 2003

ABSTRACT: Human ferritins sequester and store iron as a stable $FeOOH_{(s)}$ mineral core within a protein shell assembled from 24 subunits of two types, H and L. Core mineralization in recombinant H- and L-subunit homopolymer and heteropolymer ferritins and several site-directed H-subunit variants was investigated to determine the iron oxidation/hydrolysis chemistry as a function of iron flux into the protein. Stopped-flow absorption spectrometry, UV spectrometry, and electrode oximetry revealed that the mineral core forms by at least three pathways, not two as previously thought. They correspond to the ferroxidase, mineral surface, and the Fe(II) + H_2O_2 detoxification reactions, respectively:

$$2Fe^{2+} + O_2 + 4H_2O \rightarrow 2FeOOH_{(core)} + H_2O_2 + 4H^+ \quad (1)$$

$$4Fe^{2+} + O_2 + 6H_2O \rightarrow 4FeOOH_{(core)} + 8H^+ \quad (2)$$

$$2Fe^{2+} + H_2O_2 + 2H_2O \rightarrow 2FeOOH_{(core)} + 4H^+ \quad (3)$$

The H-subunit catalyzed ferroxidase reaction 1 occurs at all levels of iron loading of the protein but decreases with increasing iron added (48−800 Fe(II)/protein). Reaction 2 is the dominant reaction at 800 Fe(II)/protein, whereas reaction 3 occurs largely at intermediate iron loadings of 100−500 Fe(II)/protein. Some of the H_2O_2 produced in reaction 1 is consumed in the detoxification reaction 3; the 2/1 Fe(II)/H_2O_2 stoichiometry of reaction 3 minimizes hydroxyl radical production during mineralization. Human L-chain ferritin and H-chain variants lacking functional nucleation and/or ferroxidase sites deposit their iron largely through the mineral surface reaction 2. H_2O_2 is shown to be an intermediate product of dioxygen reduction in L-chain as well as in H-chain and H-chain variant ferritins.

The ferritins are ubiquitous iron mineralization proteins and play important roles in iron storage and detoxification within the cell (*1*−*4*). Mammalian ferritins are generally heteropolymers composed of 24 subunits of two types, H and L, that assemble into nearly spherical protein shells within which iron is stored as a hydrous ferric oxide mineral phase. The H- and L-subunit composition of ferritins is tissue specific, with ferritins from tissues involved in long-term storage of iron being richer in L-subunits, whereas those from tissues with more active iron metabolism have more H-subunits (*4*). The H- and L-subunits are about 50% homologous in amino acid sequence and have comparable molecular weights and tertiary structures (*3*, *4*).

The functional differences in the two types of subunits are reflected in key iron-coordinating amino acid residues. The human H-subunit contains a diiron ferroxidase center of A and B binding sites consisting of coordinating residues His65, Glu27, Glu61, Glu62, and Glu107 with Glu62 bridging the two sites (Figure 1). This center facilitates Fe(II) oxidation by dioxygen, which is followed by Fe(III) hydrolysis and mineralization to form the iron core (*1*−*6*). The H-chain also has a cluster of putative core-nucleation C-site residues, Glu61, Glu64, and Glu67, near the ferroxidase center (Figure 1). Glu61 is a shared ligand between the C- and the B-sites of the nucleation and ferroxidase centers.

The more basic L-subunit lacks a ferroxidase center. In this subunit, Glu62 is replaced by Lys to produce a salt bridge with Glu107 (*5*). The L-subunit also contains residues Glu57 and Glu60 in addition to the cluster of nucleation C-site residues Glu61, 64, 67 found in the H-subunit.[1] These additional residues along with Glu61 appear to be largely

† This work was supported by Grant R01 GM20194 from the National Institute of General Medical Sciences (N.D.C.), by the Italian Ministry of the University and Research (MURST) Cofin-2000-01 (P.A.), and by CNR Agenzia 2000 (P.A.).

* To whom correspondence should be addressed. Ph.: (603) 862-2520. Fax: (603) 862-4278. E-mail: ndc@cisunix.unh.edu.

‡ University of New Hampshire.

§ University of Brescia.

|| Protein Engineering Unit.

[1] H-chain numbering of amino acid residues is employed throughout where human H-chain numbering = L-chain numbering + 4.

10.1021/bi027357v CCC: $25.00
Published on Web 02/22/2003

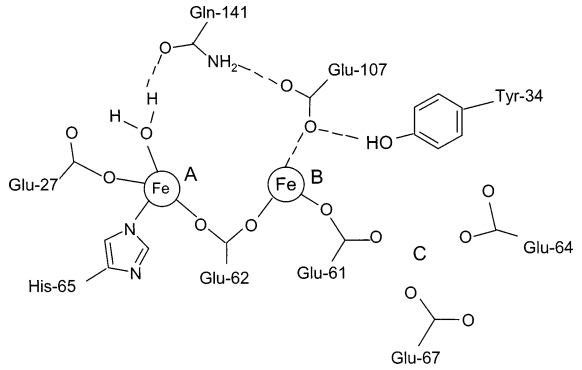

FIGURE 1: Schematic of the ferroxidase center of human H-chain ferritin. The A- and B-sites of the dinuclear iron center and the nucleation C-site are indicated.

important for mineralization in the L-chain homopolymer in vitro, albeit at a reduced rate as compared to the H-chain homopolymer HuHF (*2*, *7*, *8*). The L-chain homopolymer, HuLF, does not appear to store iron in vivo (*9*, *10*), whereas the H-chain homopolymer or mixed H/L-heteropolymers do (*9*). The ability of HuLF to incorporate Fe(III) at pH ≥ 7. 0 in vitro has been mainly attributed to autoxidation of Fe(II) (*10*).

The incorporation of iron into H-chain containing ferritins has been studied extensively in vitro. At low flux of Fe(II) into human H-chain apoferritin (HuHF)[2] (≤50 Fe(II)/protein added), the iron is essentially completely processed by the diiron ferroxidase center (*11*, *12*). The net ferroxidation/mineralization reaction occurs with an Fe(II)/O_2 stoichiometry of 2:1, resulting in the production of hydrogen peroxide according to eq 1 (*11*−*13*).

$$2Fe^{2+} + O_2 + 4H_2O + P \rightarrow \{P\text{-}[Fe_2O_2]_{FS}{}^{2+}\} \rightarrow \{P\text{-}[Fe_2O(OH)_2]_{FS}{}^{2+}\} \rightarrow P + 2FeOOH_{(core)} + H_2O_2 + 4H^+ \quad (1)$$

The above H-chain catalyzed reaction proceeds through a μ-1,2-peroxodiiron(III) intermediate, designated P-$[Fe_2O_2]_{FS}{}^{2+}$, where P represents a vacant ferroxidase site (FS) on the H-subunit. The peroxo intermediate subsequently decays to a μ-1,2-oxodiiron(III) intermediate(s) designated P-$[Fe_2O(OH)_2]_{FS}{}^{2+}$ (*14*−*21*). The fate of the H_2O_2 produced in eq 1 has been an open question because some of it is consumed in a subsequent undefined reaction(s) (*21*, *22*).

In the protein catalysis model originally proposed by Crichton and Roman (*23*), the protein is involved in oxidation of the iron(II) at all stages of core formation. This model is operable as long as the iron is delivered to the protein in small increments (<50 Fe(II)/protein) and sufficient time is allowed between additions in which case a nearly constant Fe(II)/O_2 stoichiometry of 2:1 is observed in heteropolymer and homopolymer H-chain ferritins, and the protein exhibits enzyme-like behavior (*12*, *13*, *24*). In this instance, eq 1 cycles repeatedly during mineralization of the iron core. However, when a larger flux of Fe into the protein is employed (≥200 Fe(II)/protein) the mechanism changes; the Fe(II)/O_2 stoichiometry approaches 4:1, and dioxygen is ultimately reduced to water according to the net reaction given by eq 2 (*12*, *13*).

$$4Fe^{2+} + O_2 + 6H_2O \rightarrow 4FeOOH_{(core)} + 8H^+ \quad (2)$$

Since eq 2 is identical to that for Fe(II) autoxidation and hydrolysis, it has been assumed (*12*, *13*) that core mineralization at high Fe(II) fluxes likely occurs through iron deposition directly on the surface of the mineral according to the crystal growth model (*25*, *26*). While the change in stoichiometry clearly indicates a shift in mechanism, the stoichiometric data alone are insufficient to establish eq 2 as the sole reaction for Fe(II) oxidation and mineralization at higher fluxes of Fe(II) into the protein.

In the present paper, we provide evidence for protein catalysis at both low and high iron loading of the protein and show that in addition to reaction 2, a third iron oxidation reaction involving H_2O_2 participates in core mineralization, especially during intermediate loading of the protein (100−500 Fe/protein per addition) and contributes to the rise in net Fe(II)/O_2 stoichiometry observed. Iron(II) oxidation and mineral deposition in recombinant human H-chain ferritin (HuHF), human L-chain ferritin (HuLF), a synthetic H/L-heteropolymer, and site-directed variants of HuHF were studied by UV spectroscopy, conventional and stopped-flow kinetics, and electrode oximetry. The results demonstrate that, while the Fe(II)/O_2 stoichiometry increases with increasing iron added to ferritin, indicating a shift in mechanism, the ferroxidase center continues to function in oxidizing Fe(II) at all levels of added iron but to a lesser extent as the other reactions ultimately take over. Some of the H_2O_2 produced in eq 1 is shown to react subsequently with additional Fe(II) with a stoichiometry of 2Fe(II)/H_2O_2 and contribute to formation of the core. Above 800 Fe/protein, mineralization primarily occurs through eq 2. H_2O_2 is shown to be a product of dioxygen reduction in HuLF as well as in HuHF and all H-chain variants used here.

MATERIALS AND METHODS

All chemicals were reagent grade or purer. EMPO was purchased from Oxis Research (Portland Oregon), beef liver catalase (EC 1.11.1.6), 65 000 units/mg from Boehringer-Mannheim GmbH (Germany), the Amplex Red hydrogen peroxide assay kit from Molecular Probes (Eugene, OR), ferrous sulfate from Baker Scientific Inc. of VWR Scientific (Plainfield, NJ), and Mes and Mops buffers from Research Organics (Cleveland, OH). Stock Fe(II) solutions (1−10 mM) were prepared in dilute anaerobic HCl, pH 2, solution under argon. Recombinant L- and H-chain ferritins and H-chain variants were prepared as previously described (*10*, *27*, *28*) and rendered iron-free by two anaerobic reductions using 55 and 5 mM sodium dithionite in 0.1 M Mes, pH 6.0, for 3 days each (*29*) followed by anaerobic dialysis of the protein for 2 days against 1 mM 2,2′-dipyridyl, 50 mM of MES to chelate the Fe^{2+} produced during the reduction (*30*). The resulting solution was then dialyzed against 0.1

[2] Abbreviations: EMPO, 5-ethoxycarbonyl-5-methyl-1-pyrroline-*N*-oxide; DMPO, 5,5-dimethyl-1-pyrroline-*N*-oxide; Dps, DNA binding protein from starved cells; EPR, electron paramagnetic resonance; HuHF, recombinant human H-chain wild-type ferritin; HuLF, recombinant human L-chain wild-type ferritin; HoSF, horse spleen ferritin; Mes, 2-(*N*-morpholino) ethanesulfonic acid; Mops, 3-(*N*-morpholino) propanesulfonic acid; TEMPO, 2,2,6,6-tetramethylpiperidine *N*-oxyl; A2, nucleation site variant (E61A, E64A, E67A); 222, ferroxidase center variant (E62K, H65G, and also K86Q); S1, ferroxidase plus nucleation sites variant (E61A, E62K, E64A, H65G, E67A, D42A, and also K86Q).

M Mes, 0.1 M NaCl, pH 6.0, and finally against the working buffers indicated in the figure captions. ApoHuHF concentrations were determined by absorbance at 280 nm (*21*). Other protein concentrations were determined by Advanced Protein Assay (http://cytoskeleton.com) with BSA as a standard. The synthetic H/L-heteropolymer of 30% H-chain and 70% L-chain was prepared from HuHF and HuLF as described previously (*31*). Hydrogen peroxide produced during Fe(II) oxidation in HuLF and H-chain variants was measured using the Amplex Red reagent/fluorescence assay (*21*, *32*).

The fast kinetics experiments were performed with a pneumatic drive Hi-Tech SFA-20M stopped-flow accessory on a Varian Cary 50 spectrophotometer. Equal 140 μL volumes of a weakly acidic $FeSO_4$ (pH 2.0) and buffered apoferritin solutions, both under 100% O_2 atmosphere, were mixed at 25 °C in the Peltier thermostatted sample compartment containing a quartz stopped-flow cuvette with 1 cm optical path length and cell volume of 80 μL. Unless otherwise stated, all quoted concentrations are final concentrations after mixing the two reagents. The 650 nm absorbance of the peroxo diFe(III) species formed during Fe(II) oxidation was monitored every 12.5 ms, the shortest acquisition time of the Cary 50 and the approximate deadtime of the stopped-flow apparatus. The spectrophotometer was operated in software double beam mode and zeroed prior to each kinetic run with a cuvette containing apoferritin in buffer.

The conventional ultraviolet absorption kinetic experiments of Fe(III) oxo(hydroxo) species formation were also performed on the Cary 50 spectrophotometer. The instrument was zeroed using 0.2 or 0.5 μM ferritin solution as the blank. One to 8 μL of 0.10−0.034 M $FeSO_4$ (pH 2) were injected into a 1 or 1.5 mL protein solution with rapid spin bar stirring under the conditions stated in the figure captions. Time-dependent absorbance kinetic traces at 25 °C were collected using the Cary 50 kinetic software. The kinetic data were further analyzed with Origin 6.1 software (Microcal Inc.). The initial rates of iron mineralization detected from UV absorbance changes at 305 nm were obtained from the linear A_1 term of a third-order polynomial fitted to the experimental data as described previously (*12*).

The electrode oximetry apparatus and standardization reaction for its use have been described in detail elsewhere (*12*). Fluorescence intensity for the H_2O_2 assay was measured on a Cary Eclipse fluorescence spectrometer.

RESULTS

Kinetics of Fe(II) Oxidation and Mineralization Measured by UV Spectrophotometry. UV absorption in the 300−330 nm spectral region has been traditionally used to monitor the formation of μ-oxo(hydroxo) Fe(III) species during oxidative deposition of iron in the ferritins (*12*, *29*, *35*−*37*). Spectrophotometric kinetic measurements of iron deposition in HuHF, HuLF, a synthetic H/L-heteropolymer, and three site-directed variants of HuHF were conducted to evaluate the importance of specific residues in forming the mineral core of ferritin at high iron loading of the protein (500 Fe/protein). The conventional kinetic traces obtained at 305 nm upon a single addition of 500 Fe(II) to the various protein samples and to buffer alone are shown in Figure 2. The

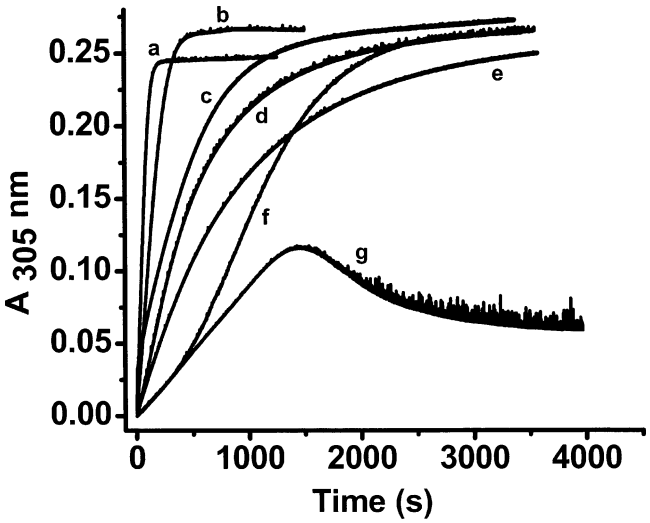

FIGURE 2: Kinetic curves for the formation of Fe(III) core following addition of 500 Fe(II) per protein. HuHF (a), $HuH_{7.2}L_{16.8}F$ (b), mutant A2 (E61A, E64A, E67A) (c), HuLF (d), mutant 222 (E62K, H65G, K86Q) (e), mutant S1 (E61A, E64A, E67A, E62K, H65G, K86Q) (f), and buffer alone (g). Conditions: 0.2 μM ferritin, 100 μM $FeSO_4$, 100 mM Mops, pH = 7.0, 25 °C.

Table 1: Specific Activities for Mineralization in Six Ferritins and in Buffer at 500 Fe(II) Added Per Protein[a]

protein	specific activity (Fe/subunit/min)	relative specific activity (%)
HuHF	43 ± 2	100
$HuH_{7.2}L_{16.8}F$	32 ± 2[b]	74[b]
nucleation site variant A2	3.0 ± 0.3	6.9
HuLF	3.1 ± 0.3	7.2
ferroxidase site variant 222	1.8 ± 0.2	4.0
ferroxidase plus nucleation sites variant S1	0.54 ± 0.25	1.2
buffer	0.38 ± 0.20[c]	0.9

[a] A molar absorptivity of 2990 M^{-1} cm^{-1} per Fe corresponding to the ferroxidase reaction was used to convert initial rates to specific activities.[3] Experimental conditions are given in Figure 2. [b] Specific activity per H-subunit. [c] The initial rate for buffer was divided by 24 times the protein concentration to scale the specific activity of the buffer to that of the proteins. All measurements were conducted at the same 100 μM Fe(II) concentration.

curves in Figure 2 follow the same general trend reported for additions of 1000 or 2000 Fe(II)/protein (*36*, *37*). HuHF (curve a) is by far the most kinetically active of the ferritins followed by synthetic $HuH_{7.2}L_{16.8}F$ (curve b). Both curves a and b are hyperbolic, consistent with protein catalysis of iron oxidation (*23*, *25*, *26*) and with these proteins having fully intact H-chain ferroxidase sites. In contrast, the curves for the other proteins (i.e., nucleation site variant A2 (E61A, E64A, E67A) (curve c), HuLF (curve d), ferroxidase site variant 222 (E62K, H65G, K86Q) (curve e), and ferroxidase plus nucleation sites variant S1 (E62K, H65G, E61A, E64A, E67A, D42A, K86Q) (curve f)) show varying degrees of sigmoidal behavior with a slow initial phase, then a second phase of increasing rate followed by a decline in rate. Such behavior is expected for an autocatalytic mineral surface mechanism (*25*, *26*). Table 1 summarizes the specific activities for mineralization calculated from the initial rates for the various proteins under the conditions in Figure 2.

Sigmoidal behavior is particularly pronounced in the ferroxidase/nucleation sites variant S1 (Figure 2, curve f). The first phase of curve f between 0 and 340 s overlaps with

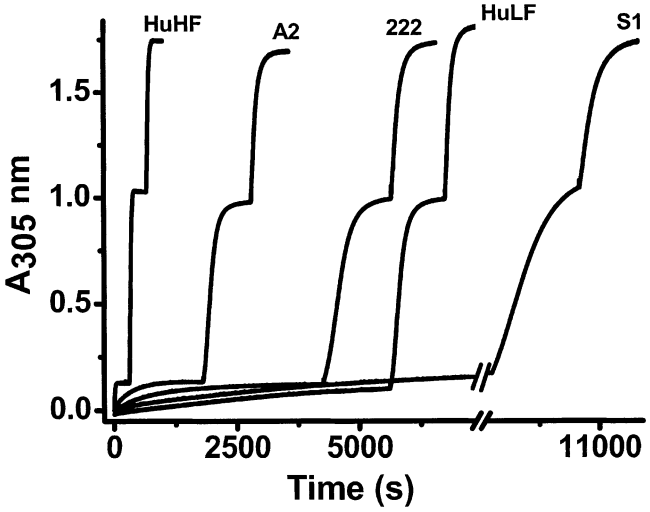

FIGURE 3: Kinetic curves for Fe(III) core formation following the sequential addition of 100, 700, and 700 Fe(II) to the protein. Conditions: 0.5 μM protein, 0.1 M Mops, 50 mM NaCl, pH 7.0.

curve g for buffer alone and is ascribed to Fe(II) autoxidation and nucleation of the $FeOOH_{(s)}$ core. The deviation between curves f and g at longer times is due to $FeOOH_{(s)}$ precipitation in the buffer solution, whereas the solution of variant S1 remains clear. The noise in curve g is due to light scattering from the formation of $FeOOH_{(s)}$ particles. We attribute the second phase beyond 340 s for variant S1 to the core surface iron oxidation/mineralization reaction (see below).

A series of additions of 100, 700, and 700 Fe(II)/protein was made to the same protein sample for a total of 1500 Fe(II) added (Figure 3). The first addition of 100 Fe(II) was intended to nucleate the iron core in each protein. Sufficient time was allowed for complete Fe(II) oxidation between each addition. The specific activities for oxo(hydroxo) Fe(III) species formation were determined from the initial rates following each addition (Table 2). A clear difference in mineralization mechanisms is evident from the data in Table 2. HuHF has a specific activity of ~40 Fe(II)/subunit/min, independent of the amount of iron added (48, 100, or 700 Fe(II)) and whether iron was present in the protein before the addition. These results indicate that the *initial* phase of the reaction is protein catalyzed for all additions of Fe(II) to HuHF. In contrast to HuHF, the specific activities for HuLF and ferroxidase site variant 222 and ferroxidase/nucleation sites variant S1 increase markedly with each increment of iron as expected for an autocatalytic mineral surface mechanism (Table 2). In contrast to these latter proteins, the specific activity for the 100 Fe(II) addition to the nucleation site variant A2 is faster than that of the first 700 Fe(II) addition, whereas the second 700 Fe(II) addition exceeds the rates of the other two (Table 2). These observations suggest some protein catalysis occurs initially in nucleation site variant A2 followed by a transition to a mineral surface mechanism with successive Fe(II) additions.

Both HuHF and $HuH_{7.2}L_{16.8}F$ showed Fe(II)/O_2 reaction stoichiometries of ~2:1 from oximetry measurements as expected for a protein ferroxidase reaction (eq 1) (*12*), whereas the stoichiometry of the nucleation site variant A2 was ~4:1 under the same conditions (48 Fe(II)/protein, 0.1 M Mops, 50 mM NaCl, pH 7). A 4:1 Fe(II)/O_2 stoichiometry also was repeatedly obtained for multiple additions of 48 Fe(II) to the same variant A2 sample (1 μM protein, pH 7) and for a single addition of either 400 or 500 Fe(II) to the protein (0.2 μM protein, pH 7). Variants 222 and S1 likewise exhibited Fe(II)/O_2 stoichiometries of 4:1 at 400 or 500 Fe(II) added.

Table 2: Specific Fe(II) Oxidation Activity of HuHF, Its Variants, and HuLF under Different Fe(II)/Protein Loading[a]

protein iron loading[b]	specific Fe^{2+} oxidation activity (Fe/subunit/min)
wild-type HuHF	
48	37 ± 6 ($N = 3$)
wild-type HuHF	
100	39 ± 3 ($N = 4$)
700	42 ± 3 ($N = 4$)
700	43 ± 2 ($N = 4$)
nucleation site variant A2	
100	10 ± 2 ($N = 3$)
700	2 ± 1 ($N = 3$)
700	15 ± 2 ($N = 3$)
ferroxidase plus nucleation sites variant S1	
100	0.11 ($N = 1$)
700	1.44 ($N = 1$)
700	10.2 ($N = 1$)
ferroxidase site variant 222	
100	0.38 ($N = 1$)
700	0.8 ($N = 1$)
700	10.4 ($N = 1$)
HuLF	
100	0.08 ($N = 1$)
700	1.07 ($N = 1$)
700	15.25 ($N = 1$)

[a] Experimental conditions are given in Figure 3. Fe(II) increments were added successively to the same protein sample. *N* is the number of determinations. [b] Iron loadings are Fe/24mer protein shell.

The unexpected Fe(II)/O_2 stoichiometry of 4:1 for the nucleation site variant A2, its reduced specific activity (Table 1), and its atypical behavior with successive additions of Fe(II) (Table 2) imply that the mutation E61A + E64A + E67A has caused a significant change in the ferroxidase center of this variant. Therefore, a careful UV spectrometric titration was carried out to measure the stoichiometry of initial Fe(II) binding and oxidation to variant A2 as has been done previously with HuHF (*12*). Fe(II) was progressively added to the protein aerobically, and iron binding and oxidation were measured by the increase in absorbance at 300−305 nm. In contrast to HuHF where 48 Fe(II) are observed to bind and oxidize per protein (2 Fe^{3+}/ferroxidase site) (*12*), only 24 Fe(II) are seen to bind and oxidize with variant A2 (Figure 4), a result implying that one of the iron binding sites of the dinuclear ferroxidase site has been disabled in this variant. Mutation of ligand Glu61 of the B site of the diiron ferroxidase center, a ligand shared with the putative nucleation site (Figure 1), is probably responsible for the observed reduction in binding in variant A2. The faster rate of mineralization for the initial addition of 100 Fe(II) as compared to the first 700 Fe(II) added (Table 2) probably reflects some residual catalytic activity in the partially disabled ferroxidase site. For nucleation site variant A2, the molar absorptivities for the first 24 iron and the remaining iron added are 2950 and 2300 cm^{-1} M^{-1} per iron, respectively, as calculated from the slopes of the intersecting lines in Figure 4. These values compare with 2990 cm^{-1} M^{-1} per iron (48 Fe/protein) and 2140 cm^{-1} M^{-1} per iron reported for HuHF (*12*).[3]

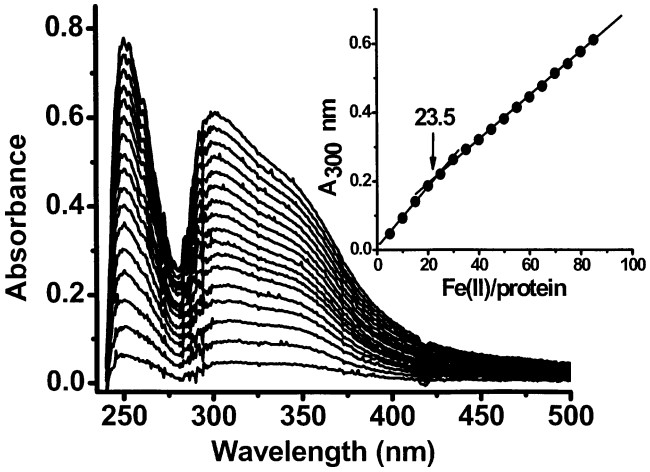

FIGURE 4: Spectrometric titration of nucleation site variant A2 (E61A, E64A, E67A) with Fe(II) aerobically. Inset: titration curve. Conditions: 3 μM protein, 0.1 M Mops, 50 mM NaCl, pH 7.0.

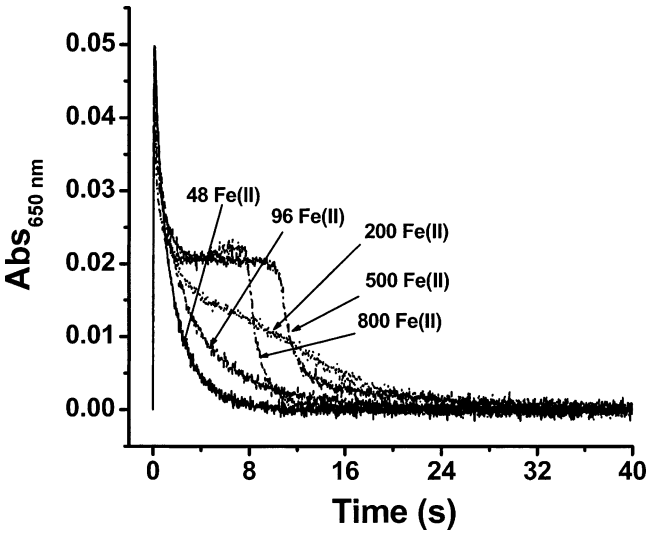

FIGURE 5: Stopped-flow measurement of formation and decay of the peroxo intermediate for different amounts of Fe(II) added to apoHuHF. Conditions: 3 μM ferritin saturated with 100% O_2, 144−2400 μM $FeSO_4$ (pH 2.0) saturated with 100% O_2, 100 mM Mops, pH = 7.0, 25 °C.

Peroxodiiron(III) Intermediate Formation. Stopped-flow spectrophotometry measurements of the production of the blue μ-peroxodiFe(III) intermediate (λ_{max} = 650 nm) were employed to directly assess the involvement of the ferroxidase pathway at different levels of iron loading of HuHF. The intermediate formed in eq 1 achieves a maximum concentration at ~160 ms following addition of Fe(II) to the protein after which it decays by a single-exponential process to form a μ-oxodiiron(III) complex(es) (*14*−*16*). This phenomenon is illustrated by the 48 Fe/HuHF curve in Figure 5 where just enough Fe(II) was added to saturate the 24 ferroxidase sites. As increasing amounts of iron (48−800 Fe/HuHF) are shot against the apoprotein in the stopped-flow apparatus, the pattern of formation and decay of the peroxo complex becomes complex. A plateau develops, indicating equal rates of peroxo complex formation and decay as iron is continually turned over at the ferroxidase site. Once all of the Fe(II) is consumed from the solution, the peroxo complex ultimately decays. These data demonstrate that the ferroxidase site continues to play some role in iron deposition

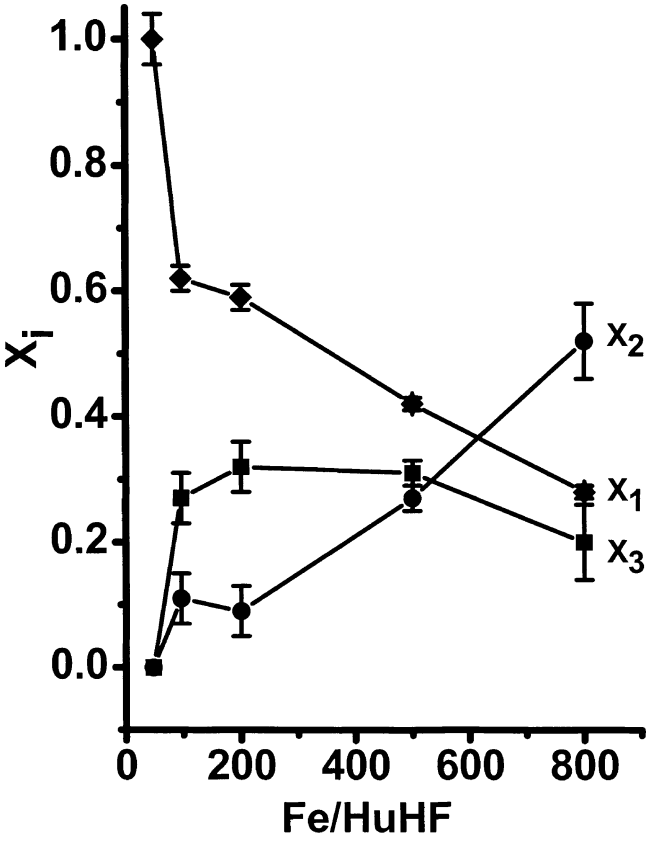

FIGURE 6: Mole fractions of iron reacting by eqs 1−3 as a function of iron loading of the protein. Conditions: 3 μM ferritin, 144−2400 μM $FeSO_4$ (pH 2.0) saturated with 100% O_2, 100 mM Mops, pH = 7.0, 25 °C.

well beyond the initial 48 Fe(II) oxidized. For example, with 500 Fe(II) added to apoHuHF, the peroxo complex is initially formed within 160 ms and continues to decay and be regenerated for ~10 s into the reaction at which time it starts to decay completely to the μ-oxo species (Figure 5). For 800 Fe(II) added, the peroxo complex is regenerated for ~8 s followed by its decay, indicating that an alternate mechanism (i.e., mineral surface) is emerging at this higher level of iron (see below).

Percentage of Fe(II) Oxidation from the Ferroxidation Reaction in HuHF. The percentage of Fe(II) oxidized by the ferroxidase reaction (eq 1) was calculated from curve fitting of the stopped-flow kinetic data of Figure 5.[4] As the amount of iron added to the apoprotein in a single shot increased from 48 to 800 Fe(II), the percentage of iron oxidized by the ferroxidase reaction 1 decreased from ~100 to ~30% (Figure 6, X_1 curve).

Oxidation of Fe(II) by H_2O_2. Figure 7 shows the dependence of the measured Fe(II)/O_2 stoichiometry on single additions of Fe(II) to HuHF samples having protein concentrations of 0.5, 1.0, and 3.0 μM under O_2 atmospheres of 21, 21, and 100%, respectively, for curves a−c. Each point represents a separate protein sample. Higher protein and iron concentrations favor slightly higher Fe(II)/O_2 stoichiometries. The inset of Figure 7 shows the dependence of the Fe(II)/O_2 stoichiometry on the Fe(II)/HuHF ratio when iron is added

[3] The previously reported molar absorptivity of 5980 M^{-1} cm^{-1} per iron was per iron dimer (*12*). The correct value is 2990 M^{-1} cm^{-1} per iron.

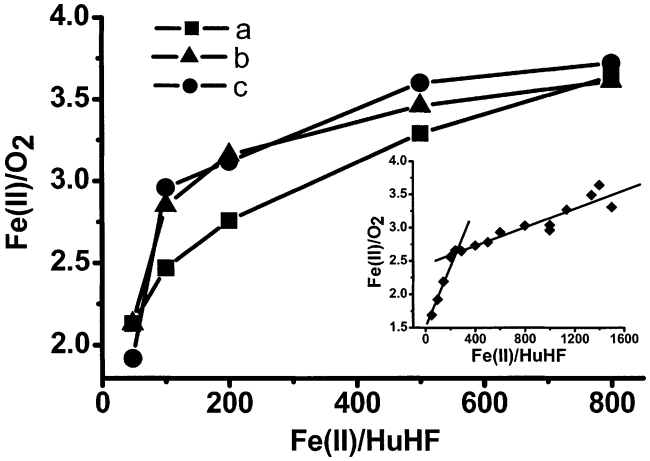

FIGURE 7: $Fe(II)/O_2$ stoichiometry as a function of iron loading of apoHuHF. Iron was added in a single addition. Curve a: 0.5 μM HuHF, 21% O_2. Curve b: 1 μM HuHF, 21% O_2. Curve c: 3 μM HuHF, 100% O_2. All curves: 9.6−2400 μM $FeSO_4$ (pH 2.0) in 100 mM Mops, pH = 7.0, 25 °C. Each point represents a different sample. Inset: $Fe(II)/O_2$ stoichiometry vs Fe(II)/HuHF for incremental addition of Fe(II) in amounts of 48, 200, 400, or 800 Fe(II)/HuHF to different protein samples and the data combined. Conditions: 0.2 μM HuHF, 0.1 M Mops, 50 mM NaCl, pH 7.0, 25 °C.

in increments of different sizes (48, 200, 500, or 800 Fe(II)/HuHF) to different protein samples and the data combined. The $Fe(II)/O_2$ stoichiometry shows biphasic behavior with added iron, the changeover occurring around 200 Fe(II)/HuHF.

The observed $Fe(II)/O_2$ stoichiometry, S, should be a simple weighted average of the 2:1 and 4:1 $Fe(II)/O_2$ stoichiometries if eqs 1 and 2 represent the only reactions occurring. The appropriate stoichiometric equation is $1/S = {}^1/_2X_1 + {}^1/_4X_2 = {}^1/_4X_1 + {}^1/_4$, where $X_1 + X_2 = 1$ and X_1 and X_2 are the mole fractions of iron oxidized by eqs 1 and 2, respectively (*12*, *13*). However, substitution of the X_1 values from the stopped-flow results (Figure 6, curve X_1) into this equation consistently predicts stoichiometries ∼20% lower than the values observed experimentally by oximetry under the same conditions (Figure 7, curve c; 96, 200, 500, or 800 Fe/HuHF, 3 μM HuHF, 0.1 M Mops, pH 7, 100% O_2 atmosphere).

The failure to predict the observed stoichiometries as well as their biphasic character with iron loading (Figure 7) implies the presence of another Fe(II) oxidation pathway not included in the calculation.[5] Fe(III) mineral cores have recently been shown to form with H_2O_2 as the Fe(II) oxidant in *E. coli* bacterioferritin (EcBFR) (*33*) and in the Dps protein (*34*), a DNA binding protein with ferritin-like properties. Therefore, the oxidation of Fe(II) by H_2O_2 was examined to determine whether the H_2O_2 produced in eq 1 is likely to react with the excess Fe(II) and contribute to core formation in HuHF. A rapid increase in absorbance at 300−305 nm was observed when 500 Fe(II) were added anaerobically to either HuHF or HuLF followed by 250 μM H_2O_2 (0.2 μM protein, 0.1 M Mops, 50 mM NaCl, pH 7.0, 25 °C). For HuHF, the rate with H_2O_2 was ∼100 times faster than with O_2 alone. When 500 Fe(II) were added to an apoHuHF solution containing both O_2 and H_2O_2 in near equal amounts, the rate of mineralization was again ∼100 times faster than that with O_2 alone (0.2 μM apoHuHF, 260 μM O_2, 250 μM H_2O_2, 0.1 M Mops, 50 mM NaCl, pH 7.0, 25 °C). These results demonstrate that H_2O_2 can efficiently compete with O_2 as the oxidant in the presence of excess Fe(II) (>48 Fe(II)/protein).

Repeated additions of 500 Fe(II) to HuLF followed by H_2O_2 up to 1500 Fe(II) total, the highest level attempted, produced a mineral core with optical properties (A_{305nm} = 3190 cm^{-1} M^{-1} per iron) similar to that observed with O_2 as the oxidant in a number of ferritins (*12*, *38*) (0.47 μM protein, 50 mM Mops, 25 mM NaCl, pH 7.5, H_2O_2/Fe(II) ratio of ∼1.4). Similar results were obtained with HuHF (A_{305nm} = 3680 cm^{-1} M^{-1} per iron). However, some $FeOOH_{(s)}$ precipitate was observed when Fe(II) was added beyond ∼400−500 Fe(II)/HuHF (250 μM Fe(II), 0.5 μM protein) in the presence of 200 μM H_2O_2, indicating that the H-chain is not as effective as the L-chain at core formation with hydrogen peroxide as the sole Fe(II) oxidant.[6]

To establish the $Fe(II)/H_2O_2$ stoichiometry for core formation with H_2O_2, anaerobic H_2O_2 spectrophotometric titrations were carried out with HuLF and HuHF samples containing 500 Fe(II)/protein. Stoichiometries of 0.47 H_2O_2/Fe(II) for HuLF (Figure 8, inset) and 0.50 H_2O_2/Fe(II) for HuHF (not shown) were obtained. Thus, two Fe(II) are oxidized per H_2O_2 reduced as previously reported for EcBFR (*33*) and Dps (*34*). The core formation reaction with H_2O_2 in HuHF and HuLF is thus given by the stoichiometric eq 3, which is the same as that found for EcBFR and Dps.

$$2Fe^{2+} + H_2O_2 + 2H_2O \rightarrow 2FeOOH_{(core)} + 4H^+ \quad (3)$$

The observed $Fe(II)/H_2O_2$ oxidation stoichiometry of 2:1 indicates pairwise oxidation of Fe(II); thus, minimal hydroxyl radical production through Fenton chemistry ($Fe^{2+} + H_2O_2 + H_2O \rightarrow FeOOH_{(s)} + HO^{\bullet} + 2H^+$) is expected, an expectation confirmed by spin trapping experiments.[7]

The stopped-flow and oximetry data were then used to estimate the fractions of iron oxidized by eqs 1−3. The net $Fe(II)/O_2$ stoichiometry S from Fe(II) oxidation through eqs 1−3 is given by $1/S = {}^1/_2X_1 + {}^1/_4X_2$ as before but in this

[4] The total amount of iron processed through the ferroxidase site mechanism was calculated from the integrated rate equations for the concentrations of the species in the sequential reaction depicted by eq 1. The kinetic analysis to be reported elsewhere (G. Zhao, F. Bou-Abdallah, H. B. Mayne, P. Arosio, and N. D. Chasteen, manuscript in preparation) indicates that the half-life for iron turnover at the ferroxidase center (i.e., decay time for the μ-1,2-oxodiFe(III) complex) is approximately 1 s at Fe(III) loadings greater than 48 Fe(II)/HuHF. Previous oximetry (*12*) and Mössbauer (*16*) studies have shown that ∼5−15 min is required for iron turnover when 48 Fe(II) or less are added to the protein. Thus, the presence of iron in excess of 48 Fe(II)/HuHF appears to greatly accelerate iron turnover at the ferroxidase center of the protein.

[5] The absorbance-time curve for 48 Fe(II) added to HuHF can be fit to a simple rising exponential of the form $A(t) = A_\infty(1 - e^{-kt})$, whereas the curve for 500 Fe(II) added cannot be adequately fit to either a single exponential or to a sum of two or three exponentials, a result consistent with multiple simultaneous/sequential reactions taking place.

[6] Analysis of the iron content of HuHF samples following dialysis typically gave iron levels between 50 and 90% of that originally added to the protein when H_2O_2 was the oxidant.

[7] EPR spin trapping experiments employing 25 mM EMPO under the conditions of these experiments have detected $HO^{\bullet}$ radical concentrations corresponding to less than 1% of the Fe(II) oxidized for samples with loadings of 48−1000 Fe/HuHF (Zhao, G., Bou-Abdallah, F., Zang, J., and Chasteen, N. D., manuscript in preparation.)

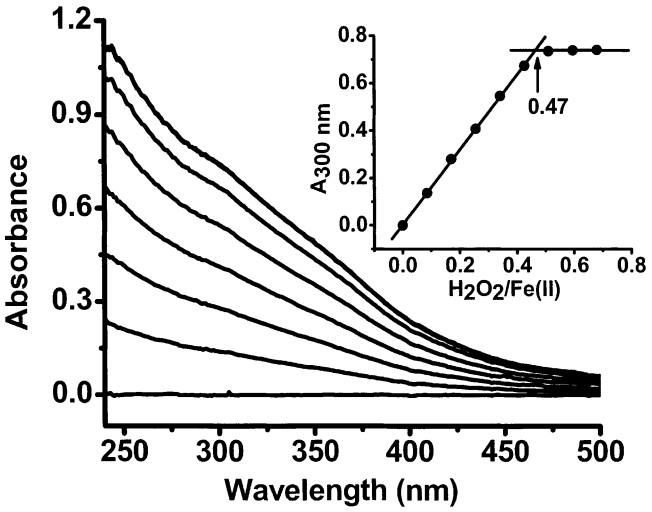

FIGURE 8: Absorption spectrum of the core of human L-chain ferritin (HuLF) as a function of added hydrogen peroxide for 500 Fe(II)/protein under argon atmosphere. Inset: spectrometric titration curve. Conditions: 0.47 μM HuLF, 50 mM Mops, 250 mM NaCl, pH 7.5, 500 Fe(II)/shell.

Table 3: Stoichiometry of Fe(II)/O_2 in HuLF at Low and High Fe(II) Loadings[a]

HuLF (2.6 μM)	stoichiometry of Fe(II)/O_2 (no catalase)	stoichiometry of Fe(II)/O_2 (catalase added prior to Fe(II))[b]
48 Fe(II)/P	2.65 ± 0.35	3.42 ± 0.17
200 Fe(II)/P	3.62 ± 0.12	4.0 ± 0.27
350 Fe(II)/P	3.99 ± 0.05	3.99 ± 0.05

[a] Conditions: 2.6 μM HuLF, 0.1 M Mops, 50 mM NaCl, pH 7.0. A total of 2 μL of 0.03−0.218 M Fe(II) was injected into 480 μL protein solution. [b] If catalase is added after Fe(II) oxidation is complete (3−5 min), no O_2 evolution is observed indicating that the stoichiometry does not change from that given in the first column. Thus, the H_2O_2 produced undergoes subsequent reactions as found for HuHF and the horse spleen ferritin (*21*, *22*).

instance $X_1 + X_2 + X_3 = 1$. By substituting $X_2 = 1 - X_1 - X_3$ into the preceding equation, we obtain an expression for the mole fraction of Fe(II) oxidized by eq 3, namely $X_3 = 1 + X_1 - 4/S$, where the value of X_1 is obtained from the stopped-flow data[4], and S is from oximetry measurements. Figure 6 shows plots of the mole fractions X_1, X_2, and X_3 for the three reactions as a function of the Fe(II)/HuHF ratio.

Stoichiometry of Iron(II) Oxidation in HuLF by O_2 and Production of H_2O_2. The stoichiometry of Fe(II) oxidation by O_2 in HuLF was measured using electrode oximetry as a function of Fe loading (Table 3). At low Fe(II) loading (48 Fe/protein, 2.6 μM HuLF), an Fe(II)/O_2 stoichiometry of 2.65:1 was observed instead of the 4:1 value expected for a mineralization reaction, indicating incomplete reduction of O_2 to H_2O. The stoichiometry increased from 2.65 to 3.42 upon addition of Fe(II) in the presence of catalase (Table 3), demonstrating that H_2O_2 is produced in HuLF. H_2O_2 production was also measured by the Amplex fluorescence method (*21*, *32*), giving a value of 1 H_2O_2 detected per 6.55 Fe(II) oxidized when 48 Fe(II)/protein were added aerobically to 0.2 μM HuLF in 0.1 M Mops, pH 7.0.

The measured Fe(II)/O_2 stoichiometry with HuLF was observed to increase from 2.65 to 3.99 with single Fe(II) additions of 48 Fe(II) to 350 Fe(II)/protein to separate samples (Table 3). In a related experiment, six injections of 50 Fe(II)/protein were made to the same 0.5 μM HuLF sample, giving increasing Fe(II)/O_2 stoichiometries of 1.99, 2.15, 2.90, 3.12, 3.47, and 3.54 as the protein progressively filled with iron. Significantly, 1 H_2O_2 per 6.95 Fe(II) oxidized was detected by the Amplex reagent cocktail when 500 Fe(II)/protein were added to 0.2 μM apoHuLF in 0.1 M Mops, pH 7.0, a result demonstrating that H_2O_2 is also an intermediate species of dioxygen reduction at high Fe(II) loading of the protein when the observed Fe(II)/O_2 stoichiometry is 4:1. Hydrogen peroxide was also detected during Fe(II) oxidation in the variants A2, S1, and 222, all exhibiting 4:1 Fe(II)/O_2 stoichiometries with 500 Fe(II) added. Stopped-flow measurements with HuLF failed to show evidence for a peroxodiiron(III) intermediate as seen with HuHF (48 Fe(II) shot against an equal volume of 5.4 μM HuLF in 0.1 M Mops buffer, pH 7.0).

DISCUSSION

The present work demonstrates that protein catalysis occurs at all stages of iron loading of human H-chain ferritin and that the hydrogen peroxide generated in the ferroxidation reaction plays a role in ferritin mineralization. While it was previously shown that iron presented to apoferritin in small increments is essentially completely processed by eq 1 (*12*, *13*, *39*), the stopped-flow data in Figure 5 indicate that the protein continues to facilitate iron oxidation even at high fluxes of Fe(II) into the protein shell but to a declining extent, accounting for only ~30% of the Fe(II) oxidized at 800 Fe(II) added (Figure 6). The decline in the ferroxidase reaction 1 with increasing Fe(II) added is immediately offset by reaction 3 involving H_2O_2 as the oxidant for Fe(II), a reaction that is most important at intermediate iron loadings of the protein (100−500 Fe/protein). Both reactions 1 and 3 are largely replaced by the mineral surface reaction 2 at 800 Fe(II)/protein (Figure 6).

The hyperbolic kinetics seen in the H-chain containing proteins, HuHF, and $HuH_{7.2}L_{16.8}F$ when 500 Fe(II) are added (Figure 2, curves a and b) can be ascribed to the initial burst in oxidation from the ferroxidase reaction 1. At this relatively high level of iron, a significant amount of oxidation still proceeds by the protein-catalyzed reaction 1 ($X_1 \cong 0.42$ in Figure 6). While the surface mineralization reaction 2 occurs to an appreciable extent at 500 Fe(II)/protein ($X_2 \cong 0.28$), its contribution to the initial phase of the reaction is masked by the fast kinetics of reactions 1 and 3. Reaction 2 presumably becomes most important in the latter phase of oxidation of the 500 Fe(II) once sufficient core has developed for autoxidation to occur appreciably on the mineral surface.

It has been previously shown that the observed increase in Fe(II)/O_2 stoichiometry beyond 48 Fe(II) added to HuHF as in Figure 7 can be simulated using a model where the first 48 Fe(II) are oxidized with a 2:1 stoichiometry (eq 1) and the remaining Fe(II) with a stoichiometry of 4:1 (eq 2) (*12*). While the simulation reproduced the observed data very well (*12*), the present work shows that this previous model of iron oxidation was incomplete. The pronounced increase in the observed Fe(II)/O_2 stoichiometry beyond 48 Fe(II)/HuHF is now more fully understood in terms of three reactions taking place. The immediate onset of reaction 3 results in consumption of much of the H_2O_2 produced in

reaction 1 and results in the sharp increase in the observed Fe(II)/O_2 stoichiometry up to 200 Fe(II)/protein (Figure 7). Note that the sum of reactions 1 and 3 equals reaction 2; thus, the effect of these two reactions on the stoichiometry is the same as if reaction 2 were occurring solely. The mineral surface reaction 2 itself begins to increase at 200 Fe(II)/HuHF (Figure 6), accounting for the more gradual rise in observed Fe(II)/O_2 stoichiometry beyond 200 Fe(II) added (Figure 7). Thus, an incipient core of 200 Fe(II) appears to be the minimal size for reaction 2 to appreciably occur.

HuLF and the variants of HuHF display sigmoidal kinetics and largely form cores by a mineral surface mechanism (Figures 2 and 3, Table 2). Iron deposition in the variant S1 (ferroxidase plus nucleation site altered) appears to be particularly representative of a mineral surface process. This variant lacks all known residues thought to be directly involved in iron oxidation or mineralization and exhibits the most pronounced sigmoidal behavior of all the proteins examined when a single addition of 500 Fe(II) is made to the protein (Figure 2). The slow initial phase of the sigmoidal curve represents nucleation and development of the incipient core upon which the autocatalytic mineral surface reaction ensues. The rate of mineralization of the first 100 Fe(II) added to variant S1 is the slowest of all the proteins (Figure 3, Table 2). Sigmoidal behavior is still observed for the first increment of 700 Fe(II)/protein but is absent for the second 700 Fe(II) addition where the curve becomes hyperbolic (Figure 3). This finding suggests that a core of 800 Fe(III) is sufficient to sustain rapid iron oxidation and hydrolysis on the mineral surface. By the second addition of 700 Fe(II), the specific activity for S1 becomes comparable with those for ferroxidase site variant 222, nucleation site variant A2, and HuLF (Table 2) at which point involvement of the protein appears to be minimal for all of the proteins and reaction 2 dominates. Likewise, reaction 2 becomes most important in HuHF only when 800 Fe(II) have been added (Figure 6), again suggesting that a core of ~800 Fe(III) is required for autoxidation at the mineral surface to become the primary pathway for further growth of the core.

In the case of HuLF, at low iron loading (48 Fe(II)/protein), an Fe(II)/O_2 stoichiometry of 2.65:1 is observed (Table 3), a value nearly identical to the 2.7:1 stoichiometry reported for human liver ferritin composed of 96% L-subunits (*11*) and significantly different from the 4 Fe(II)/O_2 expected by a mineral surface mechanism (eq 2). That H_2O_2 is the product of incomplete O_2 reduction at low levels of iron loading of HuLF was confirmed by the addition of catalase (Table 3) and by the fluorescence assay for H_2O_2 (Results). The incipient cores in HuLF may lack sufficient surface area upon which Fe(II) oxidation chemistry can exclusively occur, resulting in the release of partially reduced oxygen species into the bulk solution and accounting for the Fe(II)/O_2 stoichometries of less than 4:1. The observed production of H_2O_2 at 500 Fe(II)/HuLF, even when an Fe(II)/O_2 stoichiometry of 4:1 is obtained (Results), indicates that partially reduced intermediate oxygen species are generated during the mineral surface reaction. This H_2O_2 appears to react with mineral surface adsorbed Fe(II) to ultimately produce H_2O as previously suggested (*13*), accounting for the observation of a net Fe(II)/O_2 stoichiometry of 4:1. A similar process presumably occurs in EcBFR (*33*).

The mechanism of iron deposition in ferritin in vivo is unknown but presumably involves an oxidative process since ferritin cores cannot be efficiently reconstituted unless Fe(II) and an oxidizing agent are both present (*1*−*4*, *26*). We speculate that under physiological conditions, the flux of iron into ferritin is relatively low and that the ferroxidase reaction is largely responsible for core formation, at least initially. Under these conditions, the cellular enzyme catalase is probably responsible for the disproportionation of some of the H_2O_2 produced at the ferroxidase site, whereas under conditions of iron overload, the detoxification reaction 3 involving both Fe(II) and H_2O_2 may become significant, thus helping to attenuate harmful Fenton chemistry.

In summary, the present work has further defined the key features of the mechanism of oxidative deposition of iron in ferritin and has shown that core formation minimally involves three reactions. The protein-catalyzed ferroxidase reaction is central to the rapid initiation of mineralization within the protein shell. Under conditions of moderate iron flux, the potentially toxic H_2O_2 produced at the ferroxidase center then reacts with additional Fe(II), but in a pairwise fashion, to produce H_2O and further build the core, thus minimizing the production of odd electron oxygen species. At large iron fluxes into the protein and with increasing core size, the mineral surface autoxidation reaction becomes the primary pathway for further core growth.

ACKNOWLEDGMENT

This paper is dedicated to the memory of John Kevin Grady who, during his relatively brief life, made important contributions to our knowledge of proteins of iron storage and transport. He was a wonderful colleague and devoted mentor and friend of many students and postdoctorals who worked with him over the years. He left his mark in science, but more importantly, he enriched the lives of all who were fortunate to know him.

REFERENCES

1. Chasteen, N. D., and Harrison, P. M. (1999) *J. Struct. Biol. 126*, 182−194.
2. Chasteen, N. D. (1998) *Met. Ions Biol. Syst. 35*, 479.
3. Waldo, G. S., and Theil, E. C. (1996) in *Comprehensive Supramolecular Chemistry* (Suslick, K. S., Ed.), Vol. 5, pp 65−89, Pergamon Press, Oxford, UK.
4. Harrison, P. M., and Arosio, P. (1996) *Biochim. Biophys. Acta Bio-Energetics. 1275*, 161−203.
5. Santambrogio, P., Levi, S., Arosio, P., Palagi, L., Vecchio, G., Lawson, D. M., Yewdall, S. J., Artymiuk, P. J., Harrison, P. M., Jappelli, R., and Cesareni, G. (1992) *J. Biol. Chem. 267*, 14077−14083.
6. Hempstead, P. D., Yewdall, S. J., Fernie, A. R., Lawson, D. M., Artymiuk, P. J., Rice, D. W., Ford, G. C., and Harrison, P. M. (1997) *J. Mol. Biol. 268*, 424−428.
7. Santambrogio, P., Levi, S., Cozzi, A., Corsi, B., and Arosio, P. (1996) *Biochem. J. 314*, 139−144.
8. Crichton, R. R., Herbas, A., Chavez-Alba, O., and Roland, F. (1996) *J. Biol. Inorg. Chem. 1*, 567−574.
9. Lee, J., Seo, H.-Y., Jeon, E.-S., Park, O. S., Lee, K.-M., Park, C.-U., and Kim, K.-S. (2001) *J. Biochem. Mol. Biol. 34*, 365−370.
10. Levi, S., Luzzago, A., Cesareni, G., Cozzi, A., Franceschinelli, F., Albertini, A., and Arosio, P. (1988) *J. Biol. Chem. 234*, 18086−18092.
11. Sun, S., Arosio, P., Levi, S., and Chasteen, N. D. (1993) *Biochemistry 32*, 9362−9369.
12. Yang, X., Chen-Barrett, Y., Arosio, P., and Chasteen, N. D. (1998) *Biochemistry 37*, 9743−9750.

13. Xu, B., and Chasteen, N. D. (1991) *J. Biol. Chem. 266*, 19965−19970.
14. Treffry, A., Zhao, Z., Quail, M. A., Guest, J. R., and Harrison, P. M. (1997) *Biochemistry 36*, 432−441.
15. Treffry, A., Zhao, Z., Quail, M. A., Guest, J. R., and Harrison, P. M. (1995) *Biochemistry 34*, 15204−15213.
16. Bou-Abdallah, F., Papaefthymiou, G., Scheswohl, D. S., Stanga, S., Arosio, P., and Chasteen, N. D. (2002) *Biochem. J. 364*, 57−63.
17. Perreira, A. S., Small, W., Krebs, C., Tavares, P., Edmondson, D. E., Theil, E. C., and Huynh, B. H. (1998) *Biochemistry 37*, 9871−9876.
18. Monne-Loccoz, P., Krebs, C., Herlihy, K., Edmondson, D. E., Theil, E. C., Huynh, B. H., and Loehr, T. M. (1999) *Biochemistry 38*, 5290−5295.
19. Hwang, J., Krebs, C., Huynh, B. H., Edmondson, D. E., Theil, E. C., and Penner-Hahn, J. E. (2000) *Science 287*, 122−125.
20. Jameson, G. N. L., Jin, W., Krebs, C. Perreira, A. S., Tavares, P., Liu, X., Theil, E. C., and Huynh, B. H. (2002) *Biochemistry 41*, 13435−13443.
21. Zhao, G., Bou-Abdallah, F., Yang, X., Arosio, P., and Chasteen, N. D. (2001) *Biochemistry 40*, 10832−10838.
22. Lindsay, S., Brosnahan, D., and Watt, G. D. (2001) *Biochemistry 40*, 3340−3347.
23. Crichton, R. R., and Roman, F. (1978) *J. Mol. Catal. 4*, 75−82.
24. Waldo, G. S., and Theil, E. C. (1993) *Biochemistry 32*, 13262−13269.
25. Macara, I. G., Hoy, T. G., and Harrison, P. M. (1973) *Biochem. J. 135*, 343−348.
26. Macara, I. G., Hoy, T. G., and Harrison, P. M. (1972) *Biochem. J. 126*, 151−162.
27. Levi, S., Cesareni, G., Arosio, P., Lorenzetti, R., Soria, M., Sollazo, M., Albertini, A., and Cortese, R. (1987) *Gene 51*, 269−274.
28. Santambrogio, P., Cozzi, A., Levi, S., Rovida, E., Magni, F., Albertini, A., and Arosio, P. (2000) *Protein Expression and Purification 19*, 212−218.
29. Treffry, A., Hirzmann, J., Yewdall, S. J., and Harrison, P. M. (1992) *FEBS Lett. 302*, 108−112.
30. Bauminger, E. R., Harrison, P. M., Hechel, D., Nowik, I., and Treffry, A. (1991) *Biochim. Biophys. Acta 1118*, 48−58.
31. Santambrogio, P., Levi, S., Cozzi, A., Rovida, E., Albertini, A., and Arosio, P. (1993) *J. Biol. Chem. 268*, 2744−2748.
32. Zhou, M., Diwu, Z., Panchuk-Voloshina, N., and Haughland, R. P. (1997) *Anal. Biochem. 253*, 162−168.
33. Bou-Abdallah, F., Lewin, A. C., Le Brun, N. E., Moore, G. R., and Chasteen, N. D. (2002) *J. Biol. Chem. 277*, 37064−37069.
34. Zhao, G., Ceci, P., Ilari, A., Giangiacomo, L., Laue, T. M., Chiancone, E., and Chasteen, N. D. (2002) *J. Biol. Chem. 277*, 27689−27696.
35. Treffry, A., and Harrison, P. M. (1984) *J. Inorg. Biochem. 21*, 9−20.
36. Wade, V. J., Levi, S., Arosio, P., Treffry, A., Harrison, P. M., and Mann, S. (1991) *J. Mol. Biol. 221*, 1443−1452.
37. Levi, S., Yewdall, S. J., Harrison, P. M., Santambrogio, P., Cozzi, A., Rovida, E., Albertini, A., and Arosio, P. (1992) *Biochem. J. 288*, 591−596.
38. Yang, X., Le Brun, N. E., Thomson, A. J., Moore, G. R., and Chasteen, N. D. (2000) *Biochemistry 39*, 4915−4923.
39. Sun, S., and Chasteen, N. D. (1992) *J. Biol. Chem. 267*, 25160−25166.

BI027357V